Received: 7 February 2021 | Revised: 15 April 2021 | Accepted: 13 May 2021

DOI: 10.1111/ijag.16115

INTERNATIONAL JOURNAL OF Applied Glass SCIENCE

SPECIAL ISSUE ARTICLE

Åkermanite glass microspheres: Preparation and perspectives of sinter-crystallization

Arish Dasan[1] | **Ali Talimian**[1] | **Jozef Kraxner**[1] | **Dušan Galusek**[1,2] | **Hamada Elsayed**[3,4] | **Enrico Bernardo**[4]

[1]FunGlass, Alexander Dubček University of Trenčín, Trenčín, Slovakia

[2]Joint Glass Centre of the IIC SAS, TnUAD, and FChFT STU, FunGlass, Alexander Dubček University of Trenčín, Trenčín, Slovakia

[3]Ceramics Department, National Research Centre, Cairo, Egypt

[4]Dipartimento di Ingegneria Industriale, Università degli Studi di Padova, Padova, Italy

Correspondence
Arish Dasan, FunGlass, Alexander Dubček University of Trenčín, Študentská 2, 911 50 Trenčín, Slovakia.
Email: arish.dasan@tnuni.sk and arishd82@gmail.com

Enrico Bernardo, Universita' degli Studi di Padova, Dipartimento di Ingegneria Industriale, Edificio Ex Fisica Tecnica, Via Marzolo 9, 35131 Padova, Italy.
Email: enrico.bernardo@unipd.it

Funding information
Horizon 2020 Framework Programme, Grant/Award Number: 739566; CEGLASS, Grant/Award Number: 313011R453; Vedecká Grantová Agentúra MŠVVaŠ SR a SAV, Grant/Award Number: 1/0456/20; European Regional Development; Slovak Grant Agency of Ministry of Education, Science, Research and Sport

Abstract

Glass microspheres with the exact stoichiometry of åkermanite ($Ca_2MgSi_2O_7$), one of the most promising modern bioceramics, were produced by the flame synthesis method. The distinctive high cooling rate was found to prevent the crystallization; the size of amorphous microbeads could be correlated with the size of partially crystallized precursor powders, deriving from conventional melt quenching and milling. The glass microspheres were characterized in terms of crystallization and sintering behavior, in the perspective of applications in additive manufacturing of åkermanite-based scaffolds. The results showed that merwinite ($Ca_3MgSi_2O_8$) is the primary product of glass devitrification; only in a second stage, merwinite reacts with the residual glass and yields åkermanite. The rapid crystallization, implying limited viscous flow sintering, was tested as an opportunity to create components with complex porosity distribution.

KEYWORDS

additive manufacturing, åkermanite, crystallization, glass microspheres, viscous flow sintering

1 | INTRODUCTION

Due to controllable mechanical properties and degradation rate, åkermanite ($Ca_2MgSi_2O_7$) bioceramics have received significant attention for the production of scaffolds for bone tissue engineering.[1–3] The typical route to åkermanite bioceramics consists of the sintering of powders previously prepared by sol-gel processing[4]; the thermal transformation of

silicone polymers, added with oxide fillers, may provide a valid alternative for direct synthesis,[1–2] but there are issues of phase purity may arise due to the addition of B-based fluxes.

A further alternative may be represented by a glass route, according to which a glass with stoichiometric åkermanite composition is first formed and then crystallized into the desired silicate. Åkermanite-based materials can be effectively prepared by glass melting and subsequent conversion into glass-ceramics using an appropriate heat treatment but again, in non-stoichiometric conditions (e.g., from a SiO_2–Al_2O_3–B_2O_3–MgO–CaO–Na_2O–CaF_2 system).[5] The synthesis of glass with the exact stoichiometry of åkermanite is challenging, due to the high crystallization rate, but attractive, in the perspective of obtaining scaffolds from sinter-crystallization treatments, that is, by the crystallization of powders upon viscous flow sintering of porous preforms, for example, determined by foaming or additive manufacturing ("3D printing") of the same powders, with added organic binders.[6]

Flame synthesis is a practical approach to produce micro-sized amorphous powders by applying high cooling rates and thus preventing crystallization; interestingly, the powders are nearly perfectly spherical.[7] Due to their regular shape, microspheres are more suitable for applications in additive manufacturing than conventional powders, especially due to their superior flow properties. In stereolithography-based 3D printing, the reduced mutual friction implies a decrease of the viscosity in printable particle suspensions of photocurable binders, enabling higher solid loadings, a higher UV curing depth, and improved the dimensional stability of the printed objects.[8,9] For powder-based 3D printing technologies such as powder-bed binder jetting, multi-jet fusion, selective laser sintering, or selective laser melting, the rolling of spheroids of a controlled size undoubtedly helps the material transport, in the form of a thin layer, from the powder bed platform (moving upwards) to the printing bed platform (moving downwards), improving both printing accuracy and homogeneity of heating.[10–12]

The shaping of scaffolds, using additive manufacturing methods, is just a starting point. Especially in the field of bioceramics, the properties are largely affected by the sintering conditions. On the basis of a porous preform, before sintering, the complete densification of struts is not always desirable.[1] Components with a complex pore distribution are becoming increasingly attractive for improved cell attachment, growth, and differentiation, as well as vascularization.[13,14]

The present paper is aimed at providing fundamentals of the sintering and crystallization of åkermanite glass-ceramics with stoichiometric composition, starting from glass microspheres produced by flame synthesis. The results of a preliminary additive manufacturing (AM) study are also shown.

2 | EXPERIMENTAL PROCEDURE

Åkermanite glass powders were prepared by the conventional melt quenching method, using highly pure SiO_2, $CaCO_3$ (Centralchem), and MgO (Penta) as raw materials. The powders were first homogeneously mixed using a rotating mill for 1 h, then introduced in a Pt-10% Rh crucible, and heated at 1550°C, for 2 h. After ensuring the homogeneity by repeated swirling, the melt was poured into cold water, obtaining coarse glass-ceramic fragments. These fragments were crushed into fine powders by dry ball milling (Fritsch GmbH). The powders were separated into four size fractions, 100–80, 80–63, 63–40, and 40–25 μm, by mechanical sieving (Retsch).

Glass microspheres were produced using the flame spray synthesis method.[15] The synthesis equipment is assembled vertically and comprises: (i) a powder feeder with an adjustable diaphragm, ensuring a constant flow rate of precursor particles; (ii) oxygen–methane torch operating at fuel to oxygen ratio of 5:1 with a flame temperature of ca. 2200°C; (iii) water spray quenching system located at 10 cm of the flame torch; (iv) powder collecting tank, containing distilled water. A scheme of the experimental set-up is shown in Figure 1. Irregularly shaped particles were fed to the flame spray and the synthesized particles were collected at the bottom. Glass microbeads were finally separated from the suspension medium, by microfiltration through a ceramic filter with a pore size <0.3 μm.

The mineralogical analysis was performed using an X-ray powder diffractometer (Panalytical Empyrean, Malvern Panalytical) using Cu anode ($K\alpha_1$ = 1.5406 Å and $K\alpha_1$ = 1.5444 Å) equipped with a nickel $K\beta$ filter. The high-temperature X-ray diffraction experiments were performed in the temperature range 25–1200°C, using the powder diffractometer equipped with a high-temperature cell (Anton Paar HTK 16), with Pt heating strip used as the sample holder. The temperature was increased at a constant heating rate of 10°C min^{-1}. The diffraction data were evaluated using the software High Score Plus (v.3.0.4, Malvern Panalytical) supported by Crystallographic Open Database (COD_2013). The diffraction data were analyzed using the Rietveld refinement technique by utilizing the MAUD software (University of Trento); the quantitative determinations were carried out by refining the background, lattice parameters, and average crystallite size of selected silicate phases.

The glass transition temperature and the crystallization behavior of microspheres were studied using differential scanning calorimetry; about 50 mg samples were placed in platinum crucibles and heated up to 1300°C at the constant heating rates of 5, 10, and 20°C min^{-1} using a simultaneous thermal analyzer, STA (Jupiter 449 F1, Netzsch). Ready to press granules were made by

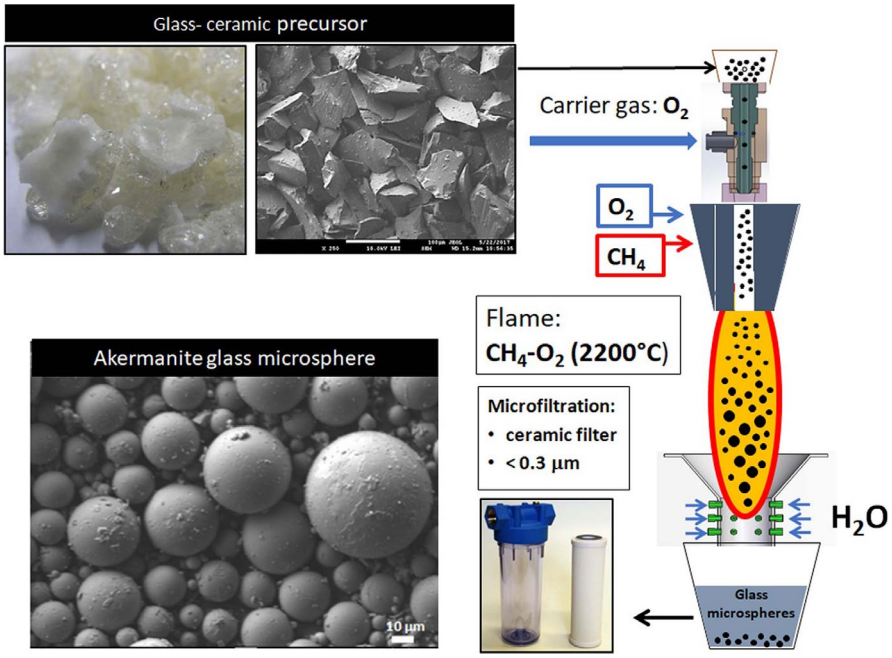

FIGURE 1 Schematic diagram of the manufacturing route for glass microspheres

adding a few drops of PVA solution (4 wt% in DI water) to the powder, mixing, and passing through a stainless steel sieve with a screen of 1 mm mesh: afterward, cylindrical pellets of 8 mm diameter, and 3–4 mm height were produced by uniaxial pressing at 20 MPa. Sintering was carried out in a thermomechanical analyzer, TMA (TMA 402 Hyperion, Netzsch) by heating the samples to 1300°C, at constant heating rates of 5, 10, and 20°C min^{-1}; pellets were located between alumina plates to ensure the uniform distribution of the applied load of 0.1 N. The morphology was examined by scanning electron microscopy (SEM, JEOL 7600 F) using an accelerating voltage of 20 kV. The semiquantitative chemical analysis was carried out using an Energy Dispersion X-Ray Spectrometer (EDS, Oxford Instruments) within Aztec systems (Oxford Instruments) with the ZAF (Z-atomic number, A-X-ray absorption, F- X-ray fluorescence) matrix correction method.

The density of glass microspheres and the final density of sintered bodies were measured following Archimedes' principle in deionized water.

The rheological properties of suspensions comprising a high-quality UV photosensitive 405 nm liquid acrylate resin (Prusa Resin-Tough, Prusa Research a.s.) and glass powders were studied by measuring the shear stress as a function of shear rate in the range of 1–450 s^{-1} at the constant temperature of 20°C using a stress-controlled rheometer (HAAKE MARS III, Thermo-Scientific). Samples with similar thermo-rheological history were produced by subjecting the suspensions to a shear rate of 450 s^{-1} for 60 s followed by a rest for 30 s before the measurements. The powders from the 40–25 µm size fraction (for both the irregular precursor powders and the microspheres) were used. Mixtures comprising 4.5 g of the photocurable organic resin for stereolithography-based 3D printing and 0.5 g of precursor powders/glass microspheres were produced.

A reticulated scaffold, with cubic cells, was manufactured by stereolithography (Original Prusa SL-1, Prusa Research s.r.o) of åkermanite microspheres in the same acrylic resin used for viscosity measurements, but for a solid loading of 60 wt%. The printer was operating in the visible light range—between 400 and 500 nm, with a layer thickness of 50 µm (exposition lasting 7 s for each layer). The firing was performed at 1000°C, for 1 h, after binder burn out (at 600°C).

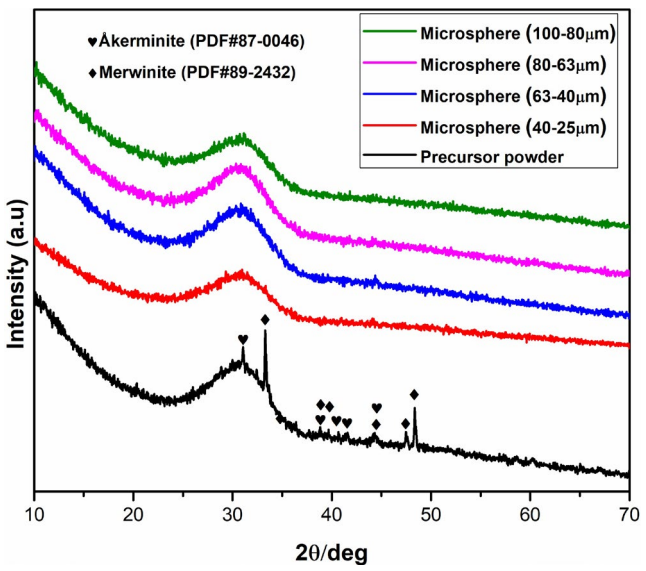

FIGURE 2 XRD patterns of precursor powders and microspheres

3 | RESULTS AND DISCUSSION

3.1 | Effect of the synthesis method

Figure 2 shows the diffraction patterns of synthesized powders, obtained by melt-quenching before and after flame synthesis. Powders with various particle sizes were used as the precursor for flame synthesis. While the diffraction pattern of the precursor powder contained peaks attributable to merwinite ($Ca_3MgSi_2O_8$) and traces of åkermanite, the flame synthesized powders were XRD amorphous. After melt-quenching, there was no diffraction peak ascribable to raw materials; this indicates that merwinite and åkermanite were formed during quenching simultaneously. The higher cooling rate of flame synthesis, compared to the conventional quenching method, was confirmed to prevent any crystallization.

3.2 | Effect of particle size and feeding rate

Figure 3 shows the SEM micrographs of glass microspheres produced from the precursor powder having a size range of 25–40, 40–63, 63–80, and 80–100 μm; the powder was fed to the flame synthesis apparatus at ~2.5, ~8.0, 15.0, and ~20.0 g min^{-1}, respectively. The flame synthesis produced spherical particles whose diameter was proportional to the initial powder size. It should be noted that the feeding rate is a crucial parameter in the production of fine microspheres, particularly <40 μm. Agglomeration of the precursor powder took place when using the fraction <40 μm. As a result, unmelted particles were detected after flame synthesis. The complete melting of precursor particles is affected by the duration of their exposure to high temperature, that is, to the "time of flight" between the combustion chamber of the torch and the water sprays. It is interesting to compare the time

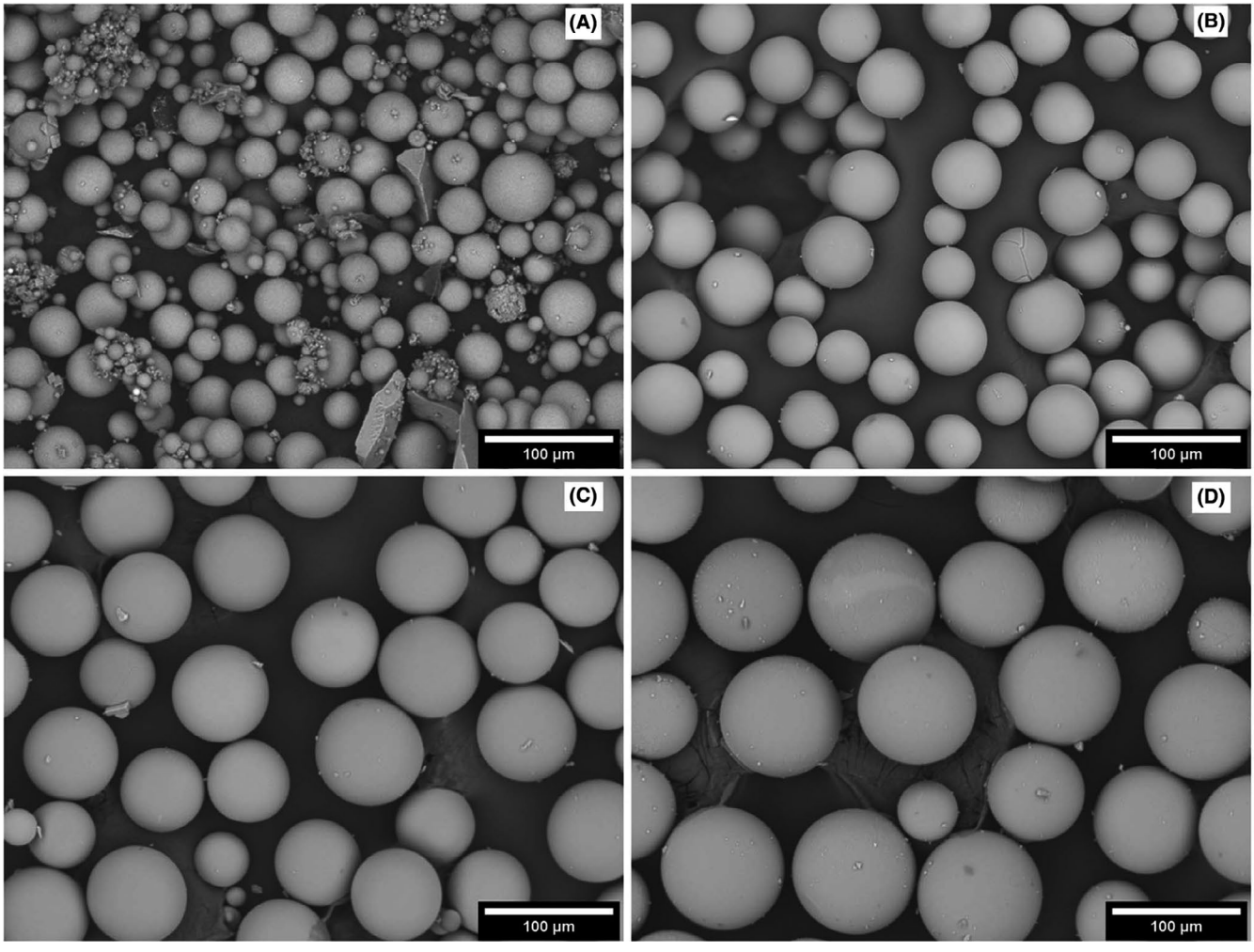

FIGURE 3 SEM micrographs of microspheres prepared from different feed particle ranges; (A) 40–25 μm, (B) 63–40 μm, (C) 80–63 μm, (D) 100–80 μm

of flight for particles with different particle sizes. We can imagine that the stream of flame exerts constant pressure on spherical particles and accelerates them; the acceleration is a function of particles radius, r, following:

$$a = \frac{3}{4} \cdot \frac{P}{\rho} r, \tag{1}$$

where P and ρ are the exerted pressure and the density of particles, respectively. Since the carrier gas pressure can be neglected compared to the flame gases, the time of flight is equal to:

$$t = \sqrt{\frac{8x}{3} \cdot \frac{\rho}{P} \cdot r}, \tag{2}$$

where x is the distance between the torch and the water sprays. Although Equation 2 is a conservative estimation, it shows that the smaller particles are exposed to the high temperature for a shorter time. For instance, particles with a diameter of 80 μm are exposed to high temperature almost twice as long as the 25 μm particles ($t^{80}/t^{25} \approx 1.8$). This may account for the partial melting of the small particles.

Table 1 shows the EDX results of the precursor powders and the corresponding representative glass microspheres. The precursor composition matched well the stoichiometry of åkermanite. No significant change in the chemical composition was observed after spheroidization.

3.3 | Crystallization kinetics

Figure 4 shows the DSC thermograms at various heating rates for as-produced microspheres [40–25 μm] between 200 and 1300°C. The first change in the base-line corresponds to the glass transition temperature (T_g) and shifts to the higher temperature with the increase of heating rate: 650 and 700°C for the samples subjected to a heating rate of 5 and 20°C min^{-1}, respectively. The DSC curves exhibited a complex exothermic peak between 800 and 900°C. In samples heated at 5°C min^{-1}, the peak is a convolution of an intense peak with peak temperature (T_p) at 820°C corresponding to the crystallization of a first phase (phase I, merwinite as evidenced by HT-XRD analysis discussed later) and a less intense one at 870°C, corresponding to the crystallization of a second phase (phase II, later identified as åkermanite). T_p shifts to higher

TABLE 1 Chemical composition of precursor powders and microspheres measured by EDX

Sample	MgO (wt%)	SiO_2 (wt%)	CaO (wt%)
Theoretical ($2CaO{\cdot}MgO{\cdot}2SiO_2$)	14.8	44.1	41.1
Precursor powder	15.9 ± 0.5	44.3 ± 0.2	39.8 ± 0.3
Microspheres from sieved precursor (100–80 μm)	15.2 ± 0.4	44.5 ± 0.3	40.3 ± 0.5
Microspheres (80–63 μm)	15.6 ± 0.5	43.7 ± 0.2	40.7 ± 0.3
Microspheres (63–40 μm)	15.4 ± 0.3	43.6 ± 0.1	41.0 ± 0.2
Microspheres (40–25 μm)	15.6 ± 0.4	43.6 ± 0.3	40.8 ± 0.4

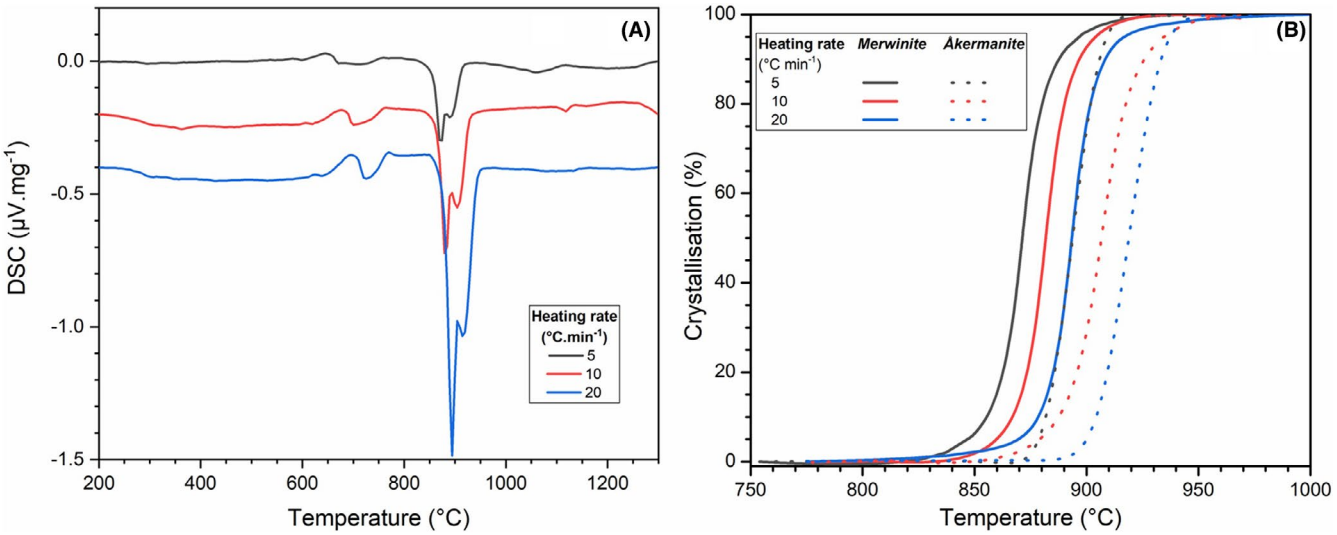

FIGURE 4 (A) DSC curves of microspheres subjected to heating to 1300°C using constant heating rates of 5, 10, and 20°C min^{-1}; (B) crystallization fractions (%) estimated from the DSC peaks

temperatures and becomes stronger when higher heating rates are used. No other significant events were detected by heating the samples to 1300°C.

The crystallization behavior of samples was further studied by determining the fraction of crystallized phases as a function of temperature, T; the complex peak was deconvoluted by assuming it as composed of two crystallization peaks and fitted by Voigt function; then, the crystallization fraction, X, was determined using:

$$X(T) = \frac{\int_{T_C}^{T} J(T)\,dT}{\int_{T_C}^{T_E} J(T)\,dT} \times 100, \quad (3)$$

where J is the heat flow recorded by DSC measurements, and T_C and T_E are the crystallization temperature and the final temperature of the crystallization, respectively. Figure 4B shows the crystallization fraction for phase I and phase II at different heating rates as a function of temperature.

Using the analogy of the crystallization curves with the densification progress during sintering, and by assuming that a single mechanism is responsible for crystallization of each phase, master kinetic curves, MKC, can be constructed to determine the apparent activation energy of crystallization.[16,17] The MKC equation is given by

$$\psi(X) = \theta(t, T). \quad (4)$$

where $\psi(X)$ includes the crystallization fraction and is assumed to be independent of temperature and time. The parameter $\theta(T, t)$, which includes time and temperature-dependent terms, is given as:

$$\theta(T,t) = \int_{t_0}^{t} \frac{1}{T} \exp\left(\frac{-Q_{app}^{Cry}}{RT}\right) dt. \quad (5)$$

where $Q_{app}{}^{cry}$ is the apparent activation energy of crystallization, t and t_0 being the time and time corresponding to the glass transition temperature. The master kinetic curves were constructed following the approach reported by Torrens-Serra et al.[16] Figure 5 shows the rate of crystallization fraction against $\log\theta$ and the estimated apparent activation energy of crystallization for phase I and phase II.

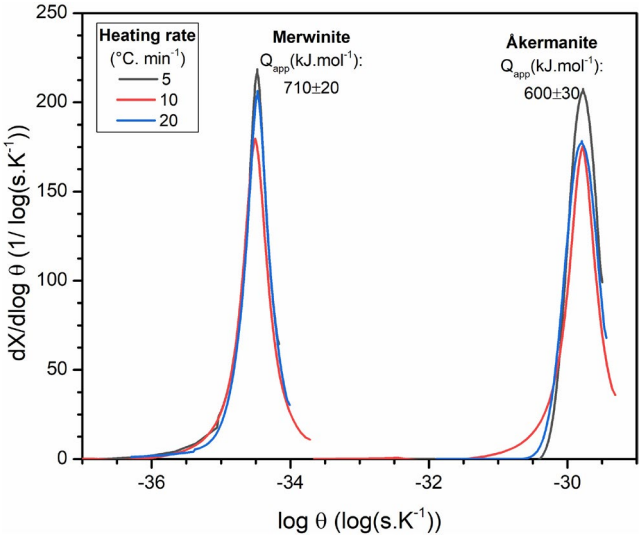

FIGURE 5 Estimated crystallization rates (dX/d log θ) calculated using the master kinetic curve approach, and corresponding "apparent activation energy of crystallization" of phase I and phase II

3.4 | Densification

Figure 6A shows the linear shrinkage of the pellets as a function of temperature upon heating at a constant rate of 5, 10, and 20°C min^{-1}. The first shrinkage of pellets occurred at ~250°C and is related to the binder burn out and water evaporation; samples exhibit a relatively slow shrinkage followed by a rapid one at a temperature above the glass transition temperature, 650°C. The former is due to the "first shrinkage" as termed by Pascual et al.,[18] and the latter is a result of densification by viscous flow. The shrinkage curve reaches a plateau at ca. 850°C; the onset temperature of events shifts to the higher temperature when higher heating rates are used.

Table 2 summarises the relative density and open porosity of the samples produced by heating up to 1300°C at different heating rates.

Figure 6B shows a representative example of the polished cross-section of a pellet subjected to heating up to 1300°C at a constant heating rate of 5°C min^{-1}. Although the touching area (early-stage neck growth) has grown significantly (h/d ≈0.5), the shape and radius of spheres remained unchanged during the sintering; this allows treating the microspheres as linear viscous materials during the sintering. Moreover, the viscosity of glass can be expressed as an Arrhenius function of temperature:

$$\eta(T) = \eta_0 \cdot e^{\frac{Q}{RT}}. \quad (6)$$

By considering the similarity of the viscosity correlation with temperature to that of material diffusion, $D = D_0 \cdot e^{-Q/RT}$, the concept of master sintering curve can be extended to the viscous flow, Equations 4 and 6, to determine the activation energy of the viscous flow.[19,20] To this end, the instantaneous density of samples was calculated using the dilatometry results following the approach reported by Pouchlyet al.,[21] and assuming the samples undergo isotropic shrinkage. Then, the master sintering curve was constructed following the method

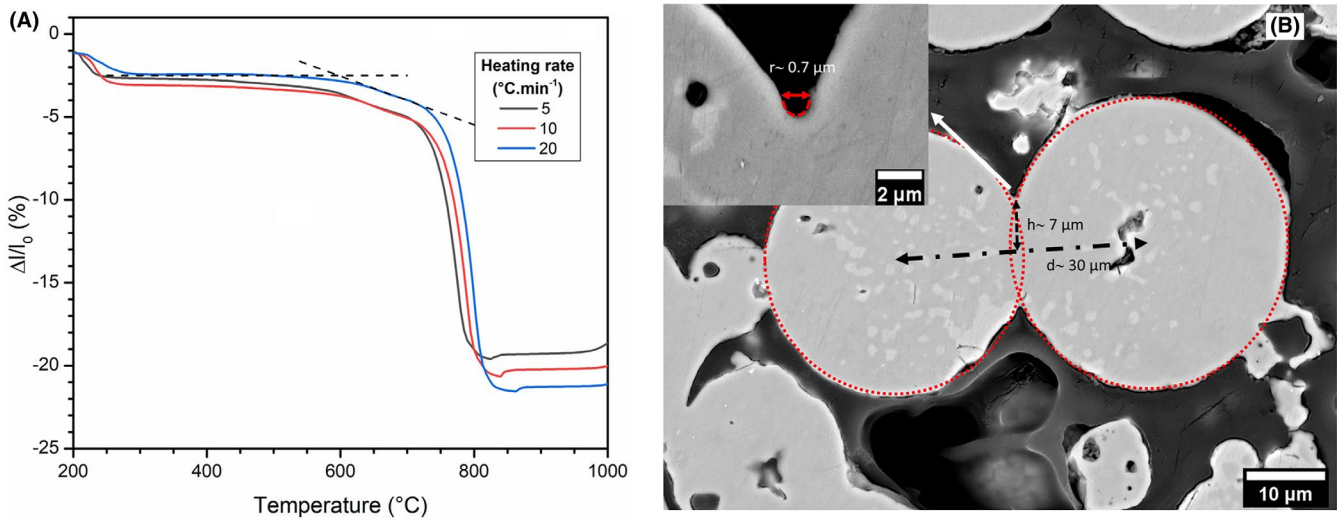

FIGURE 6 (A) Shrinkage of pellets subjected to heating at constant rates of 5, 10, and 20°C min^{-1} to 1300°C; (B) cross-section of bodies sintered at 1300°C using the heating rate 5°C min^{-1} (radius of spheres, *r*: 15 µm and the neck radius: 7 µm)

TABLE 2 Relative density, calculated with respect to the theoretical density (2.6 g cm^{-3}), and open porosity of samples subjected to conventional sintering by heating to 1300°C at 5, 10, and 20°C min^{-1}

Heating rate (°C)	Relative density (%)	Open porosity
5	59.8 (0.4)	22.5 (0.3)
10	63.2 (0.7)	19.6 (0.9)
20	63.8 (0.3)	19.2 (0.4)

The numbers between parentheses represent the measurement error.

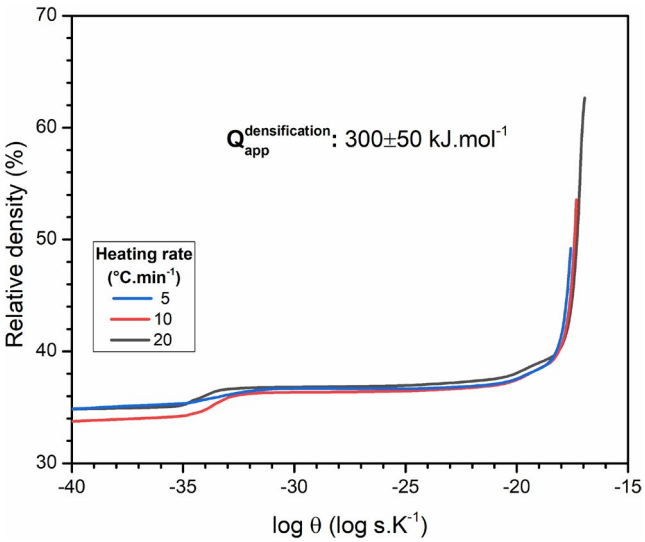

FIGURE 7 Master sintering curve calculated for samples heated to 1300°C at 5, 10, and 20°C min^{-1}

described elsewhere.[22–24] Figure 7 illustrates the master curve developed for sintering of samples below 850°C (before crystallization). The apparent activation energy of sintering is then estimated to be 300 kJ mol^{-1}, which is in good agreement with the activation energy for the viscous flow of glasses with a similar composition.[25]

3.7 | Rheological properties of the suspensions of glass microspheres

The effect of particles shape on the rheological properties of glass powder/resin mixtures was quantified in terms of specific viscosity, η_{sp}:

$$\eta_{sp} = \frac{\eta}{\eta_0} - 1. \quad (7)$$

where η is the viscosity of the suspension, and η_0 the viscosity of the resin. Figure 8 shows shear stress as a function of shear rate obtained from rheological experiments for suspensions comprising of microspheres or irregular-shape particles at 20°C. The measured data for the photocurable organic resin are also shown for comparison. All samples exhibited an almost perfectly linear Newtonian behavior, but the suspension containing irregular particles was characterized by a higher viscosity. The specific viscosity of the suspension with irregular glass particles was close to $\eta_{sp} = 0.4$. The use of microspheres led to a specific viscosity of ca. 0.1, confirming the assumption that the use of microspheres improves the flowability of the suspension; this undoubtedly encourages the fabrication of architected structures with macroscopic porosity.

Preserving the produced pores during sintering is a prerequisite for the fabrication of hierarchical porosity required

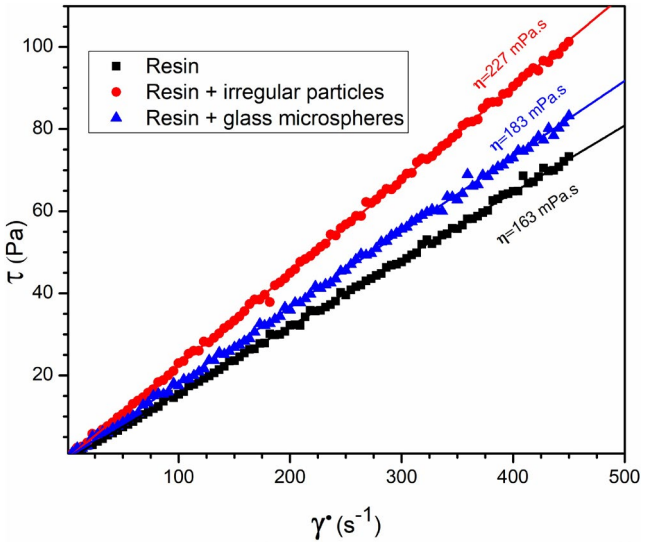

FIGURE 8 Shear stress vs shear strain rate curves of glass-filled photocurable resin

for bone tissue engineering.[26] The sintering kinetics of glass-ceramics is affected by (i) the crystallization of glass and (ii) the densification of the green body due to viscous flow.

3.8 | Phase evolution and preliminary AM test

The previously mentioned phases, phase I and phase II, were identified as merwinite ($Ca_3MgSi_2O_8$, COD#99-900-0226) and åkermanite ($Ca_2MgSi_2O_7$, COD#99-900-0178), respectively. Merwinite was dominant at lower temperatures, according to "dynamic" mineralogical analysis, shown in Figure 9A and B (samples heated at 10°C min^{-1} and left for 18 min at each temperature step). At 850°C, the formation of åkermanite could be appreciated only after 30 min (isothermal study in Figure 9C). Merwinite probably originated from CaO-richer zones, and its formation was kinetically favored by its simpler crystal structure, comprising "insular" SiO_4 groups surrounded by Ca^{2+} and Mg^{2+} ions,[27] compared

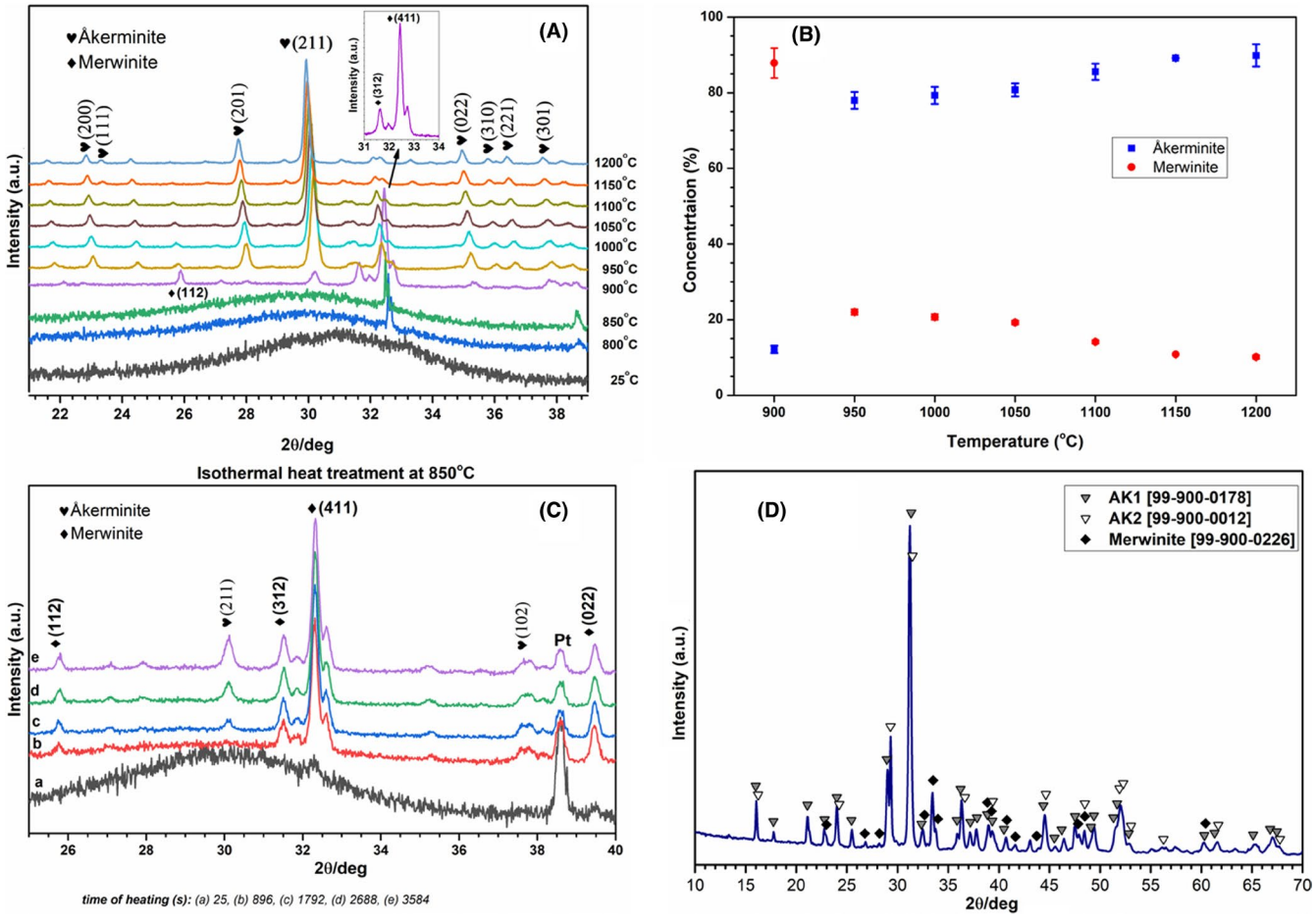

FIGURE 9 Mineralogical analysis of microspheres after sintering: (A and B) at increasing heating temperature; (C) for several holding times at 850°C (D) for 1 h at 1000°C

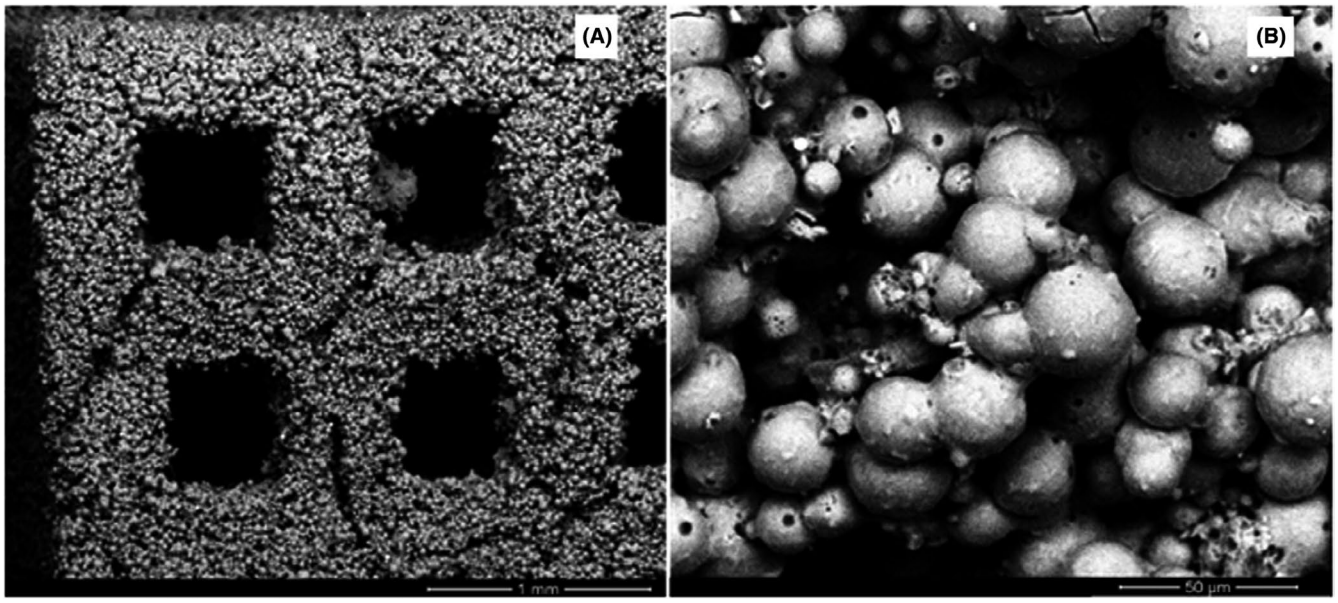

FIGURE 10 Example of a cubic-celled 3D scaffold (A) from sinter-crystallization of åkermanite microspheres at 1000°C, for 1 h, with evidence of interstitial voids (B)

with that of åkermanite, known to correspond to the sandwiching of Ca^{2+} ions between Mg-silicate sheets.[28] In other words, the glass microspheres evolved, with firing temperature and firing times, toward the conditions of thermodynamic stability (crystal phase of the same stoichiometry), by ionic interdiffusion.

The preliminary separation of merwinite within an Mg-silicate residual glass matrix, can be seen as a key condition for the "freezing" of viscous flow, with the stabilization of shrinkage, already at about 850°C, in agreement with the results of the TMA analysis, showing an abrupt end of densification at $T > 800$°C (Figure 6A). From the perspective of tissue engineering applications, the presence of merwinite cannot be considered an issue, since also this phase is recognized as an excellent biomaterial.[27]

An example of the possible exploitation of the freezing of viscous flow operated by crystallization in the manufacturing of scaffolds with multiform porosity is illustrated by Figure 10. According to the rheological study, glass microspheres could be used, suspended in photocurable resin, in high amounts, and shaped by stereolithography into a reticulated scaffold with cubic cells. The high solid loading, in maximizing the packing, prevented an extensive sliding of particles after debinding; the crystallization, upon firing at 1000°C, prevented the coarsening of particles and the viscous collapse of struts. A total porosity of 73%, completely open, derived from the overlapping of macropores of the geometrical model adopted for printing (Figure 10A) and interstitial micropores (Figure 10B).

The adopted sintering temperature (1000°C), supported by a relatively long holding time (1 h), determined an inversion in the proportion between silicates, with merwinite much less abundant compared to åkermanite (Figure 9D). The latter likely formed in two polymorphic variants (besides COD#99-900-0178, also in the variant described by COD#99-900-0012).

Future work will be dedicated to variation of printing conditions (processing parameters, scaffold geometry) and sintering conditions (temperature, duration, heating rate), for the generation of a multitude of åkermanite-based porous bioceramics.

4 | CONCLUSIONS

The main findings of this study can be summarized as follows:

- A homogeneous glass with åkermanite ($Ca_2MgSi_2O_7$) stoichiometry cannot be obtained by conventional melt quenching process, owing to the remarkable devitrification tendency of the system, upon cooling;
- The partially crystallized material from the cooling of an åkermanite melt, finely powdered, can be considered feedstock for the obtainment of fully amorphous microspheres by flame synthesis; for the precursor powder fraction below 40 µm, particle agglomeration could be avoided only when operating at a low feeding rate (<2.0 g min^{-1}). Larger precursor powder particles allowed a high feeding rate (up to ~20.0 g min^{-1}, for 100–80 µm fraction of the precursor powder);
- The spherical shape of microspheres effectively led to an improvement in the fluidity of resin/particle suspensions, to be used in additive manufacturing applications;

- A careful study of the crystallization of the microspheres confirmed the formation of merwinite ($Ca_3MgSi_2O_8$) as a preliminary phase in the system devitrification;
- The crystallization of åkermanite glass may be exploited for controlling the viscous flow sintering; highly porous scaffolds for bone tissue applications may easily feature macroporosity from printing, as well as many additional interstitial pores between adjacent particles, from incomplete densification.

ACKNOWLEDGMENTS

This paper is a part of the dissemination activities of project FunGlass (Center for Functional and Surface Functionalized Glass). This project has received funding from the European Union´s Horizon 2020 research and innovation program under grant agreement No 739566. This publication was also created in the frame of the project Center for Functional and Surface Functionalized Glass (CEGLASS), ITMS code is 313011R453, operational program Research and innovation, co-funded from the European Regional Development Fund. Authors also gratefully acknowledge the financial support from Slovak Grant Agency of Ministry of Education, Science, Research and Sport, VEGA 1/0456/20. The authors are grateful to Dr. Si Chen and Dr. Michal Žitňan for their experimental assistance (flame synthesis and HT-XRD).

ORCID

Arish Dasan https://orcid.org/0000-0002-5550-6776
Dušan Galusek https://orcid.org/0000-0001-5995-8780
Hamada Elsayed https://orcid.org/0000-0002-9818-4498
Enrico Bernardo https://orcid.org/0000-0003-4934-4405

REFERENCES

1. Dasan A, Elsayed H, Kraxner J, Galusek D, Colombo P, Bernardo E. Hierarchically porous 3D-printed åkermanite scaffolds from silicones and engineered fillers. J Eur Ceram Soc. 2019;39:4445–9. https://doi.org/10.1016/j.jeurceramsoc.2019.06.021
2. Dasan A, Elsayed H, Kraxner J, Galusek D, Colombo P, Bernardo E. Engineering of silicone-based mixtures for the digital light processing of åkermanite scaffolds. J Eur Ceram Soc. 2020;40:2566–72. https://doi.org/10.1016/j.jeurceramsoc.2019.11.087
3. Dong X, Li H, Lingling E, Cao J, Guo B. Bioceramic åkermanite enhanced vascularization and osteogenic differentiation of human induced pluripotent stem cells in 3D scaffolds in vitro and vivo. RSC Adv. 2019;9:25462–70. https://doi.org/10.1039/C9RA02026H
4. Wu C, Chang J, Zhai W, Ni S, Wang J. Porous akermanite scaffolds for bone tissue engineering: preparation, characterization, and in vitro studies. J Biomed Mater Res Part B: Appl Biomater. 2006;78B:47–55. https://doi.org/10.1002/jbm.b.30456
5. Ventura JMG, Tulyaganov DU, Agathopoulos S, Ferreira JMF. Sintering and crystallization of akermanite-based glass–ceramics. Mater Lett. 2006;60:1488–91. https://doi.org/10.1016/j.matlet.2005.11.059
6. Schmidt J, Elsayed H, Bernardo E, Colombo P. Digital light processing of wollastonite-diopside glass-ceramic complex structures. J Eur Ceram Soc. 2018;38:4580–4. https://doi.org/10.1016/j.jeurceramsoc.2018.06.004
7. Bernardo E, Fiocco L, Prnová A, Klement R, Galusek D. Gehlenite:Eu^{3+} phosphors from a silicone resin and nano-sized fillers. Opt Mater. 2014;36:1243–9. https://doi.org/10.1016/j.optmat.2014.03.007
8. Li W-D, Wang C, Jiang Z-H, Chen L-J, Wei Y-H, Zhang L-Y, et al. Stereolithography based additive manufacturing of high-*k* polymer matrix composites facilitated by thermal plasma processed barium titanate microspheres. Mater Des. 2020;192:108733. https://doi.org/10.1016/j.matdes.2020.108733
9. Xu X, Zhou S, Wu J, Zhang Q, Zhang Y, Zhu G. Preparation of highly dispersive solid microspherical α-Al_2O_3 powder with a hydrophobic surface for stereolithography-based 3D printing technology. Ceram Int. 2020;46:1895–906. https://doi.org/10.1016/j.ceramint.2019.09.167
10. Fateri M, Gebhardt A. Selective laser melting of soda-lime glass powder. Int J Appl Ceram Technol. 2015;12:53–61. https://doi.org/10.1111/ijac.12338
11. Sofia D, Barletta D, Poletto M. Laser sintering process of ceramic powders: the effect of particle size on the mechanical properties of sintered layers. Addit Manuf. 2018;23:215–24. https://doi.org/10.1016/j.addma.2018.08.012
12. Datsiou KC, Saleh E, Spirrett F, Goodridge R, Ashcroft I, Eustice D. Additive manufacturing of glass with laser powder bed fusion. J Am Ceram Soc. 2019;102:4410–4. https://doi.org/10.1111/jace.16440
13. Zirak N, Jahromi AB, Salahinejad E. Vancomycin release kinetics from Mg–Ca silicate porous microspheres developed for controlled drug delivery. Ceram Int. 2020;46:508–12. https://doi.org/10.1016/j.ceramint.2019.08.290
14. Ma N, Ma B, Zhou Y, Zhu H, Zhou Y, Huan Z, et al. In vivo evaluation of the subchronic systemic toxicity of åkermanite bioceramic for bone regeneration following ISO standard methods. RSC Adv. 2019;9:17530–6. https://doi.org/10.1039/C9RA02496D
15. Kraxner J, Masar V, Timar Š, Chovanec J. Úžitkový vzor/Utility model: Zariadenie na výrobu plných, dutých alebo pórovitých sklených alebo sklo-keramických mikroguľôčok pomocou plameňovej syntézy/Flame synthesis device for the production of solid, hollow and porous glass and glass-ceramics microspheres, číslo/No. 8673. 2020, Slovak Republic.
16. Torrens-Serra J, Venkataraman S, Stoica M, Kuehn U, Roth S, Eckert J. Non-isothermal kinetic analysis of the crystallization of metallic glasses using the master curve method. Materials (Basel). 2011;4(12):2231–43. https://doi.org/10.3390/ma4122231
17. Chan TV, Shyu GD, Isayev AI. Master curve approach to polymer crystallization kinetics. Polym Eng Sci. 1995;35(9):733–40. https://doi.org/10.1002/pen.760350902
18. Pascual MJ, Pascual L, Duran A. Determination of the viscosity–temperature curve for glasses on the basis of fixed viscosity points determined by hot stage microscopy. Phys Chem Glasses. 2001;42(1):61–6.
19. Mohanram A, Messing GL, Green DJ. Densification and sintering viscosity of low-temperature co-fired ceramics. J Am Ceram Soc. 2005;88(10):2681–9. https://doi.org/10.1111/j.1551-2916.2005.00497.x
20. Wadsworth FB, Vasseur J, von Aulock FW, Hess K-U, Scheu B, Lavallee Y, et al. Nonisothermal viscous sintering of volcanic ash. J Geophys Res Solid Earth. 2014;119(12):8792–804. https://doi.org/10.1002/2014JB011453
21. Pouchly V, Maca K. Master sintering curve – a practical approach to its construction. Sci Sinter. 2010;42:25–32. https://doi.org/10.2298/SOS1001025P

22. Frueh T, Ozer IO, Poterala SF, Lee H, Kupp ER, Compson C, et al. Messing GL.A critique of master sintering curve analysis. J Eur Ceram Soc. 2018;38(4):1030–7. https://doi.org/10.1016/j.jeurceramsoc.2017.12.025
23. Su H, Johnson DL. Master sintering curve: a practical approach to sintering. J Am Ceram Soc. 1996;79:3211–7.
24. Pouchlý V, Maca K, Boccaccini A. Sintering densification curve – a practical approach for its construction from dilatometric shrinkage data. Sci Sinter. 2008;40:117–22. https://doi.org/10.2298/SOS0802117M
25. Hrma P, Han S-S. Effect of glass composition on activation energy of viscosity in glass-melting-temperature range. J Non Cryst Solids. 2012;358(15):1818–29. https://doi.org/10.1016/j.jnoncrysol.2012.05.030
26. Minas C, Carnelli D, Tervoort E, Studart AR. 3D printing of emulsions and foams into hierarchical porous ceramics. Adv Mater. 2016;28:9993–9. https://doi.org/10.1002/adma.201603390
27. Ou J, Kang Y, Huang Z, Chen X, Wu J, Xiao R, et al. Preparation and in vitro bioactivity of novel merwinite ceramic. Biomed Mater. 2008;3:015015. https://doi.org/10.1088/1748-6041/3/1/015015
28. Swainson IP, Dove MT, Schmahl WW, Putnis A. Neutron powder diffraction study of the åkermanite-gehlenite solid solution series. Phys Chem Miner. 1992;19:185–95. https://doi.org/10.1007/BF00202107

How to cite this article: Dasan A, Talimian A, Kraxner J, Galusek D, Elsayed H, Bernardo E. Åkermanite glass microspheres: Preparation and perspectives of sinter-crystallization. *Int J Appl Glass Sci*. 2021;12:551–561. https://doi.org/10.1111/ijag.16115